

TILT OBSERVATIONS USING BOREHOLE TILTMETERS  
 2. ANALYSIS OF DATA FROM YELLOWSTONE NATIONAL PARK

Charles Meertens,<sup>1</sup> Judah Levine, and Robert Busby<sup>2</sup>

Joint Institute for Laboratory Astrophysics,  
 National Bureau of Standards and University of Colorado, Boulder

**Abstract.** We have installed borehole tiltmeters at five sites in Yellowstone National Park, Wyoming, and have used these instruments to measure the spatial variation of the amplitude and phase of the principal semidiurnal tide. The measured tides vary both with position and azimuth and differ from the sum of the body tide and the ocean load by up to 50%. The difference predicted by a finite element model constructed from seismic, refraction, and gravity data has a maximum value of only 12%, although the discrepancy between our observations and the model is only marginally significant at some sites. The disagreement between the model and our observations is much larger than we observed using the same instruments at other sites and cannot be attributed to an instrumental effect. We have been unable to modify the model to explain our results while keeping it consistent with the previous observations.

Introduction

In paper 1 [Levine et al., this issue], we described a deep borehole tiltmeter design and tidal analysis procedures. An array of these tiltmeters was installed in Yellowstone National Park, Wyoming. We used the instruments to measure the amplitude and phase of the Earth tides at five locations in the park. In this paper we compare these measurements with the prediction of a finite element model of the region.

Beaumont and Berger [1974] showed that the amplitude and phase of the Earth tides would vary with position near the boundary between regions of different elastic parameters or seismic velocities. They estimated that a 10% contrast in  $V_p$  might produce a change of up to 40% in the amplitude of the tides. This effect would be largest near the velocity discontinuity and would be of comparable magnitude for either tilt or strain observations.

This effect is caused by a coupling between strain and tilt near the boundary. In equilibrium, stress is continuous across the

boundary, and the strains on either side will therefore be different. The discontinuity in strain gives rise to tilts which decrease with distance from the boundary. These strain-induced tilts also couple strain tides and tilt tides, which results in a spatially varying tidal admittance.

The coupling between strain and tilt would also produce a secular tilt in response to a secular strain, and the observed uplift in Yellowstone might therefore be at least partially a response to secular strain. We will discuss this issue later.

Elastic parameters such as Poisson's ratio or the bulk modulus do not completely specify the strain-tilt coupling, as can be seen from the simplified models of Harrison and Flach [1976] and Harrison [1978] (see Figure 1). All of the models had the same 10% contrast in  $V_p$  between the interior and exterior zones, but the bulk modulus and Poisson's ratio differed. The models were (1) a body extending to 100 km with material properties corresponding to very flat inclusions, (2) the same body with round inclusions, and (3) a body with the same material properties as model 1 but extending to a depth of 200 km. Models 1 and 3 have a lower modulus and a higher Poisson's ratio than model 2. Depending on how far from the boundary the measurement is made, the amplitude of the tides changes by up to 40% for models 1 and 3 but is considerably smaller for model 2. Under favorable circumstances, a measurement of the tides can thus serve to discriminate among models that have the same contrast in  $V_p$ .

Previous Investigations

Yellowstone National Park has recently been the site of a large number of geophysical and geological investigations, many of which are summarized by Eaton et al. [1975] and by Smith and Christiansen [1980]. The results of these investigations suggest the presence of a large, hot, and possibly molten body beneath the center of the park. The body has been studied using many different techniques: gravity surveys show a large low-density mass beneath the park; magnetic surveys show a low value, suggesting that the Curie depth may be only about 10 km beneath the surface as compared with an average Curie depth of 15-30 km for the continental United States. There are also seismic anomalies: P waves travel about 15% slower in the crustal portion of the body and up to 5% slower in the deeper portions down to about 250 km; S waves are absent from some ray paths traversing the area, suggesting that at least part of the body is molten.

These and other investigations are consistent

<sup>1</sup>Now at Department of Geology and Geophysics, University of Utah, Salt Lake City.

<sup>2</sup>Now at Lamont-Doherty Geological Observatory, Palisades, New York.

Copyright 1989 by the American Geophysical Union.

Paper number 88JB03599.  
 0148-0227/89/88JB-03599\$05.00

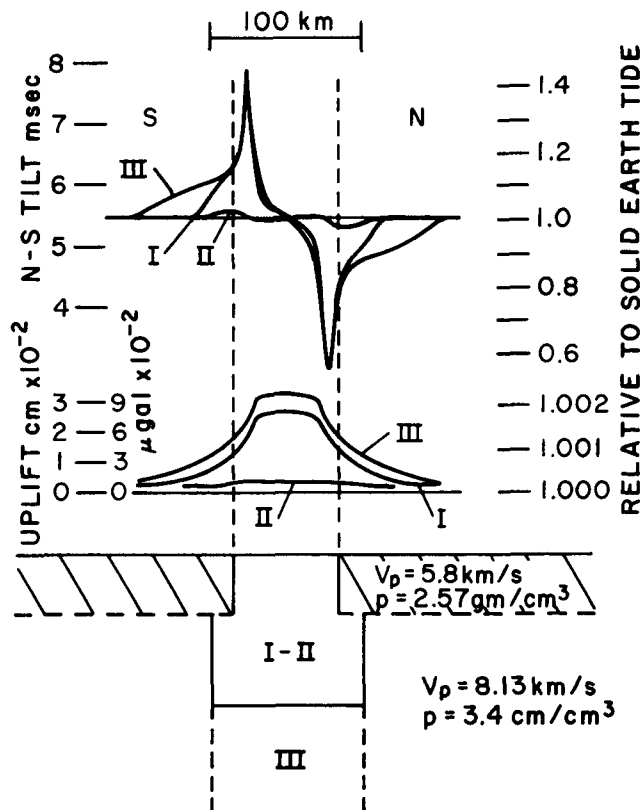


Fig. 1. Axially symmetric finite element models of Harrison [1978]. All three models are consistent with the observed reduction of 10% in  $V_p$ . Models 1 and 3 have round inclusions which give a lower modulus and a higher Poisson's ratio than the flat inclusions of model 2.

with a 40 km  $\times$  60 km collapsed caldera with a low-density, hot, and mechanically weak region below it [Lehman et al., 1982]. Newly acquired uplift data from repeat gravity and line level surveys, seismic refraction data, and geologic data have been interpreted by Smith and Braile [1984] to indicate the possibility of volcanic activity in the future. Such activity would not be unique in the region; quaternary volcanism was both extensive and voluminous.

#### Instrument Sites

The sites were chosen to be close to the edges of the anomalous zone as defined by Eaton et al. [1975], Smith et al. [1982], and others, since the strain-tilt coupling is largest there. The site at Lake is near the southeastern edge of the caldera; Canyon, Norris, and Madison are all at road junctions on the northwest edge of the caldera; Tower was intended as a control station away from the anomalous body (see Figure 2). The location of the boundary of the low-velocity zone is different in some of the newer seismic models that were completed after the instruments had been installed [Smith and Braile, 1984], and in these models, Tower is close to the edge of the anomalous region. The coordinates of the sites

and the details of the installation and operation are given in paper 1.

#### Data Acquisition and Analysis

The first reliable data were recorded early in 1983, and the analysis included data through June 1986. The data from each borehole were analyzed in blocks, most of which were about 3000 hours long (30,000 values at 10 samples/h). The two sensors in each borehole were analyzed independently using the methods outlined in paper 1. The amplitude and phase of the  $M_2$  tidal component were estimated by a least squares fit of the tidal potential to a data set from which the secular tilt had been removed using our spline estimator. The uncertainty of the amplitude estimate was computed from the measured signal-to-noise ratio in each data set: the ratio of the  $M_2$  power to the power in the residuals of the least squares fit at the same frequency.

The signal-to-noise ratios for a 1-month data set varied from over 40 dB at Canyon to 23 dB at Lake. The high noise level in the tidal bands at Lake and a quasi-periodic signal with a period of 54 min recorded there may be due to seiches from nearby Yellowstone Lake. The secular tilt rate at Lake was also particularly large and ranged up to 2  $\mu$ rad/yr.

In Table 1 we show the measured amplitudes and phases of the  $M_2$  tidal component for all of the data sets. There were several blocks of data with the same azimuth at most sites, and these estimates are shown separately and are then averaged together. For each block of data, the azimuth of the instrument is given, the  $M_2$  amplitude in nrad, the phase with respect to the local tidal potential in degrees (phase lags are negative), the length of the block in hours and the starting date of the block. The "ident" column gives the source of the data set. The entry for BH specifies which of the two boreholes at each site was used, TM gives the tiltmeter serial number, and PN specifies one of the two pendulums in the tiltmeter. The uncertainty in each amplitude is computed from the signal-to-noise ratio of the data set as described above. If the noise is uncorrelated with the tides, an uncertainty of 1% in amplitude implies an uncertainty of 0.6° in phase.

The estimates in Table 1 are used to construct amplitude and phase estimates along azimuths of 45° and 315° using linear combinations of pairs of phasors. We combined data from orthogonal pendulums whenever possible; the constituents of each estimate are shown in column 2 of Table 2. Except at Norris, where only one azimuth was used, the projected estimates are averaged with weights proportional to the lengths of the data sets used in their construction (see Table 2). The uncertainties are the standard deviations of the average amplitudes and are somewhat higher than would be computed from the signal-to-noise ratios of the constituent time series.

The body tide and the ocean load should be the same at all of the stations, since they are less than 50 km apart. The ocean load is computed using the ocean models of Parke [1978] and Schwiderski [1980]. The two load estimates differ by about 30% in amplitude. The average of

## Hebgen Lake - Yellowstone Region

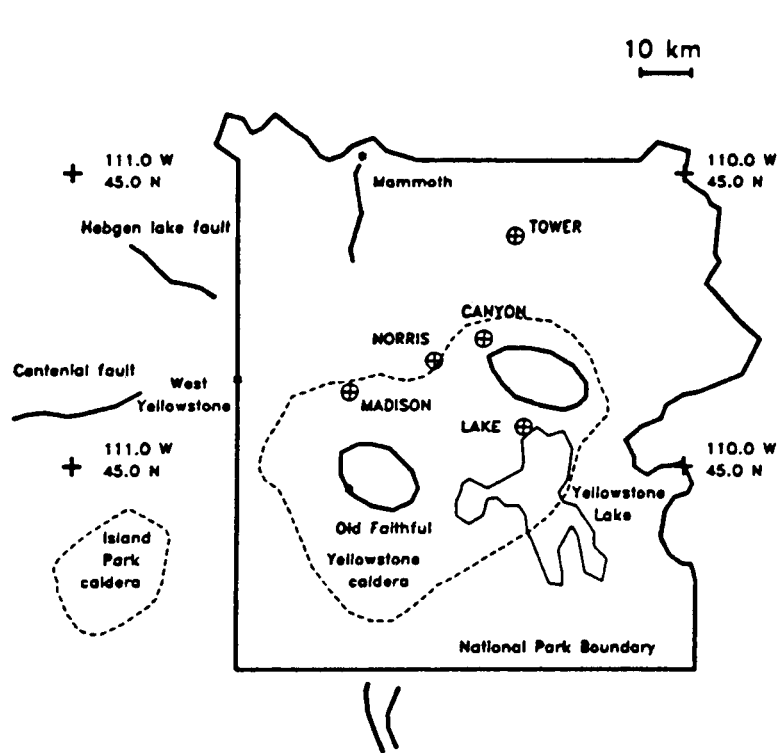


Fig. 2. Map of the Yellowstone region showing the locations of the tiltmeter sites. The edge of the caldera is shown by a dashed line, with the two resurgent domes shown by heavy solid lines.

the two estimates is combined with the body tide, as shown in Table 3. The 30% difference in the two ocean load estimates translates into a 5% uncertainty in the combined estimate along  $45^\circ$  and a 10% uncertainty along  $315^\circ$ .

A comparison of Tables 2 and 3 shows significant differences at all of the stations except Canyon, where the disagreement is roughly equal to the uncertainty of the measurement. The largest discrepancy is at Norris, where the measured tide along an azimuth of  $315^\circ$  is only about 55% of the theoretical value.

The variation does not exhibit a simple pattern as would be expected from the cylindrical model of Figure 1, and we constructed a finite element model using the material properties deduced from previous work to explain our results. The failure of the cylindrical model of Figure 1 to explain our data is not due only to its lack of detail; the cylindrical model solutions have discontinuities and singularities at the boundary between the low-velocity and normal zones, and these effects dominate the predicted response.

Singularities exist both in finite element and analytic solutions for any model with a sharp discontinuity in elastic parameters. Bogy [1968] found an analytic solution for the stresses between two edge-bonded, orthogonal isotropic wedges. The solution for the stress has a weak singularity at the free edge-bond intersection. Christensen [1979] attempted to solve the same problem using finite element methods, but the

solution did not converge for any mesh size. The derivatives of the displacements were singular, and the tilts asymptotically approached  $90^\circ$  at the boundary.

These unphysical results arise in a fundamental way from the sharply defined boundary conditions, and they can only be avoided by using a larger, smoother model with smaller contrasts between adjacent elements. The size of the model should be limited by the spatial resolution of the input data.

#### Previous Yellowstone Models

The elastic material properties for this study are a synthesis of existing geophysical models, primarily seismic velocity models. Individually, these models either do not completely define the elastic parameters or they do not adequately resolve the geologic structure. We have combined the S wave velocity structure of Daniels and Boore [1982], the teleseismic P wave velocity structure of Iyer [1979] and Iyer et al. [1981], the refraction models of Lehman et al. [1982] with the model of Evoy and Smith [1979].

The Evoy-Smith model is the result of a simultaneous inversion of the teleseismic P wave delays and surface gravity measurements. The inversion showed a low-density body centered under the caldera that was 60 km wide at the surface widening to 150 km at a depth of 100 km.

This type of inversion has the poorest resolu-

TABLE 1a. M<sub>2</sub> Tidal Amplitude and Phase: Canyon Site-Yellowstone Tilt Array

Azimuth, deg	Amplitude, nrad	Error, %	Phase, deg	Length, hours	Ident B T P H M N	Start Date
318	28.45	0.5	-131.4	2867	1 3 1	Feb. 26, 1983
48	32.73	1.0	113.5	2867	1 3 2	Feb. 26, 1983
152	25.11	1.5	42.0	3015	1 1 2	Aug. 10, 1983
152	25.12	1.6	42.0	2928	1 1 2	Dec. 14, 1983
Average	25.12		42.0			
62	33.69	1.0	111.4	3039	1 1 1	Aug. 10, 1983
62	33.69	1.1	108.4	2900	1 1 1	Dec. 15, 1983
Average	33.69		109.9			
85	36.90	1.3	83.4	3180	2 3 1	Aug. 4, 1983
85	37.63	1.2	81.4	3119	2 3 1	Dec. 15, 1983
85	37.99	1.5	82.4	2472	2 3 1	Oct. 7, 1984
85	35.18	2.0	81.4	1780	2 3 1	Jan. 18, 1985
Average	36.93		82.2			
175	28.44	2.0	-8.0	3180	2 3 2	Aug. 4, 1983
175	28.09	2.0	-8.0	3119	2 3 2	Dec. 15, 1983
175	28.03	1.0	-1.4	2472	2 3 2	Oct. 7, 1984
175	26.45	2.0	-8.0	1800	2 3 2	Jan. 18, 1985
Average	27.75		-6.4			
285	37.13	0.5	-102.8	3176	2 3 2	Sept. 15, 1985
285	37.57	1.0	-101.2	1500	2 3 2	Jan. 24, 1986
Average	37.35		-102.0			
195	34.04	2.0	-14.0	3176	2 3 1	Sept. 15, 1985
195	33.43	1.8	-13.0	1520	2 3 1	Jan. 24, 1986
Average	33.74		-13.5			

tion in the upper 10-15 km of the crust, so that the refraction and gravity results of Lehman et al. [1982] are used to define that portion of the structure.

The S wave velocities also constrain the

elastic properties. These are not well resolved by the existing studies, and our estimate of the spatial dependence of these velocities has the greatest uncertainty of any component of the model. Since Daniels and Boore give only a

TABLE 1b. M<sub>2</sub> Tidal Amplitude and Phase: Tower Junction-Yellowstone Tilt Array

Azimuth, deg	Amplitude, nrad	Error, %	Phase, deg	Length, hours	Ident B T P H M N	Start Date
4	22.94	2.1	166.7	2053	1 2 1	Sept. 20, 1983
4	22.43	2.0	166.1	3024	1 2 1	Dec. 15, 1983
4	23.67	2.1	166.3	1080	1 2 1	April 27, 1984
Average	23.01		166.4			
94	32.84	2.5	97.9	3177	1 2 2	Aug. 4, 1983
94	36.49	2.0	97.7	3048	1 2 2	Dec. 15, 1983
Average	34.67		97.8			
306	30.00	2.4	-96.2	910	1 1 2	Jan. 18, 1983

TABLE 1c. M<sub>2</sub> Tidal Amplitude and Phase: Lake Site-Yellowstone Tilt Array

Azimuth, deg	Amplitude, nrad	Error, %	Phase, deg	Length, hours	Ident B T P H M N	Start Date
103	28.10	5.6	96.8	2890	1 4 1	Feb. 28, 1985
193	10.29	7.0	-32.2	2000	1 4 2	Jan. 18, 1984
193	9.34	6.9	-35.2	3192	1 4 2	Oct. 10, 1984
193	8.71	6.9	-31.2	1400	1 4 2	July 11, 1985
193	9.61	7.1	-41.2	2300	1 4 2	Nov. 13, 1985
Average	9.49		-34.9			
255	31.08	2.2	-95.4	1093	2 0 1	Oct. 16, 1983
255	31.86	2.0	-92.4	1600	2 0 1	Jan. 18, 1984
Average	31.47		-93.9			
260	35.80	1.6	-86.0	2800	2 0 1	Sept. 23, 1984
260	34.93	1.5	-84.4	2500	2 0 1	Jan. 18, 1985
Average	35.36		-85.2			
350	13.01	6.4	-177.9	3200	2 0 2	Sept. 7, 1984
350	12.23	6.3	-173.9	2000	2 0 2	Jan. 18, 1985
Average	12.62		-175.9			

horizontal average for this velocity, we did not incorporate the lateral gradation in elastic constants shown in the models of Iyer et al. [1981].

The model can be specified using only Young's modulus and Poisson's ratio, but deriving these parameters from the seismic velocity profile requires the density as well. Gravity data provide the average density, but not its vertical profile. We follow Daniels and Boore [1982] in confining the low-density region to the upper 10 km of the crust.

We tested the sensitivity of our results to the properties of the uppermost low-velocity layer, which is 2.5 km thick. Although the stress and strain near the surface are very sensitive to the parameters of the top layer, the effect on a tiltmeter is dominated by the Pg layer in the upper crust (layer 2 of our model). This layer is characterized by a velocity of 5.7 km/s in the zone of interest in contrast to 6.05 km/s in the surrounding material. This low-velocity region roughly coincides with the caldera rim and the gravity low and has been

TABLE 1d. M<sub>2</sub> Tidal Amplitude and Phase: Madison Site-Yellowstone Tilt Array

Azimuth, deg	Amplitude, nrad	Error, %	Phase, deg	Length, hours	Ident B T P H M N	Start Date
157	27.93	1.0	56.1	1403	1 1 2	Sept. 20, 1984
157	26.59	1.5	57.1	3191	1 1 2	Nov. 18, 1984
157	26.07	1.2	57.1	1488	1 1 2	March 31, 1985
Average	26.86		56.8			
67	29.90	2.2	116.6	1288	1 1 1	Sept. 25, 1984
67	28.43	2.2	114.4	3191	1 1 1	Nov. 18, 1984
67	29.35	2.1	115.6	1488	1 1 1	March 31, 1985
Average	29.23		115.5			
2	22.81	1.1	-123.8	1900	1 2 2	Sept. 23, 1985
272	32.93	1.1	-64.4	3185	1 2 1	Sept. 14, 1985
272	33.09	1.1	-70.4	3143	1 2 1	Jan. 25, 1986
Average	33.01		-67.4			

TABLE 1e.  $M_2$  Tidal Amplitude and Phase: Norris Site-Yellowstone Tilt Array

Azimuth, deg	Amplitude, nrad	Error, %	Phase, deg	Length, hours	Ident B T P H M N	Start Date
204	34.80	2.7	-64.4	3180	1 5 1	Oct. 5, 1984
204	34.87	2.9	-63.4	1600	1 5 1	Feb. 15, 1985
204	34.80	3.0	-66.9	2891	1 5 1	July 10, 1985
204	36.09	3.1	-65.9	2879	1 5 1	Nov. 8, 1985
204	36.75	3.0	-65.9	1590	1 5 1	March 8, 1986
Average	35.46		-65.3			
294	22.56	3.4	-123.2	3180	1 5 2	Oct. 5, 1984
294	22.65	3.4	-120.2	3191	1 5 2	Feb. 15, 1985
294	22.65	3.6	-124.2	3191	1 5 2	June 28, 1985
294	22.93	4.0	-123.2	3191	1 5 2	Nov. 8, 1985
294	22.84	3.8	-123.2	1944	1 5 2	March 21, 1986
Average	22.73		-122.8			

TABLE 2.  $M_2$  Tidal Amplitudes and Phases Rotated to Azimuths of  $45^\circ$  and  $315^\circ$ 

Station	Using	$45^\circ$ Azimuth		$315^\circ$ Azimuth	
		Amplitude, nrad	Phase, deg	Amplitude, nrad	Phase, deg
Canyon	318+48	32.08	115.9	29.18	-128.4
Canyon	152+62	30.23	122.9	29.19	-119.8
Canyon	175+85	33.07	114.8	32.25	-139.0
Canyon	285+195	35.09	134.4	36.09	-129.9
Weighted average ( $\pm 4\%$ )		33.00	122.0	31.20	-128.2
Tower	94+4	33.27	126.9	25.00	-117.0
Tower	306+4	37.65	128.7	26.48	-105.4
Weighted average ( $\pm 5\%$ )		33.50	127.1	25.00	-117.0
Lake	103+193	21.12	113.3	20.83	-93.6
Lake	260+350	29.92	108.8	22.65	-112.3
Lake	255+350	25.77	100.2	22.45	-122.8
Weighted average ( $\pm 7\%$ )		25.50	110.0	21.60	-100.0
Madison	157+67	23.50	137.0	31.99	-106.2
Madison	272+2	19.22	158.9	35.22	-89.0
Weighted average ( $\pm 4.5\%$ )		22.40	142.0	32.50	-100.0
Norris ( $\pm 2.5\%$ )	204+294	38.00	104.0	18.10	-160.0

TABLE 3. M<sub>2</sub> Theoretical Tides for Yellowstone National Park

Theory	Azimuth, deg	Amplitude, nrad	Phase, deg
Body	45	33.24	125.0
Body	315	33.24	-125.0
Ocean Load(s)	45	3.82	-145.3
Ocean Load(p)	45	5.27	-127.2
Ocean Load(s)	315	6.94	-30.6
Ocean Load(p)	315	9.40	-29.1
Combined	45	32.90	132.9
Combined	315	33.52	-111.0

Note that (s) uses the ocean model of Schwiderski [1980]; (p) uses the model of Parke [1978]. The combined entry uses the average of the two load estimates.

interpreted to be of granitic composition [Lehman et al., 1982].

Within the 5.7 km/s region are two smaller zones with V<sub>p</sub> = 4 km/s. The northeast zone coincides with a gravity low and may be the site of a shallow partial melt. The southwest body,

YELLOWSTONE ANOMALOUS BODY  
3-D FINITE ELEMENT MODEL - VIEW FROM SOUTH

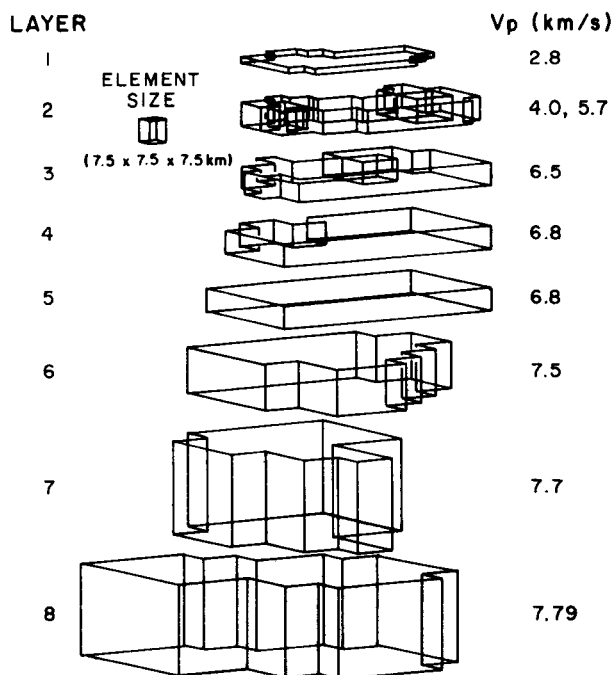


Fig. 3. An exploded-view diagram of the three-dimensional model used for this study. Only the outlines of the elements are shown. The two very low modulus bodies in the upper crust are outlined with bold lines in layer 2.

TABLE 4. Elastic Parameters of Anomalous Section Model YEL7C

Layer	V <sub>p</sub> , km/s	V <sub>s</sub> , km/s	ρ, kg/m <sup>3</sup>	E, GPa	ν
1	2.80	1.62	2400	15.68	0.25
2L	4.00	1.62	2400	17.92	0.40
2	5.70	2.74	2650	53.65	0.35
3	6.50	3.12	2700	71.08	0.35
4	6.80	3.27	2700	77.79	0.35
5	6.80	3.64	2700	92.74	0.30
6	7.50	4.33	2700	126.56	0.25
7	7.70	4.45	2700	133.40	0.25
8	7.79	4.50	2700	136.54	0.25

which was present in the earlier models, does not coincide with a gravity low and is absent from the most recent models.

There is a significant discrepancy between the teleseismic and refraction models at an intermediate (10-20 km) depth and for the lower crust (20-40 km) [Smith and Braile, 1984; Smith et al., 1982]. The teleseismic results give a velocity reduction of 15-20% in a single layer that includes both the upper and intermediate layers and a 10% reduction in the lower crust. The refraction results [Smith et al., 1982] show low velocities in the intermediate crust but near normal velocities in the lower crustal layer.

Three-Dimensional Model

The axes of the finite element model were chosen to lie along azimuths of 45° and 315° so that the y axis was aligned with the long axis of the caldera. The dimensions of the model were 210 km x 210 km x 140 km deep. The model had eight vertical layers, with thicknesses of 2.5, 10, 10, 10, 10, 20, 40, 40 km from top to bottom. The deeper elements are larger because their contribution to the result decreases rapidly with depth. The model contained 6272 elements and 9251 nodes. The top two layers were composed of rectangular elements, 7.5 km on a side. The elements had 12 nodes each, one at each corner

TABLE 5. Elastic Parameters of Reference Section Same for All Models

Layer	V <sub>p</sub> , km/s	V <sub>s</sub> , km/s	ρ, kg/m <sup>3</sup>	E, GPa	ν
1	4.50	2.60	2600	43.88	0.25
2	6.05	3.49	2700	82.26	0.25
3	6.05	3.49	2700	82.26	0.25
4	6.80	3.93	2700	104.19	0.25
5	6.80	3.93	2700	104.19	0.25
6	7.90	4.56	2700	140.38	0.25
7	7.90	4.56	2700	140.38	0.25
8	7.95	4.59	2700	142.21	0.25

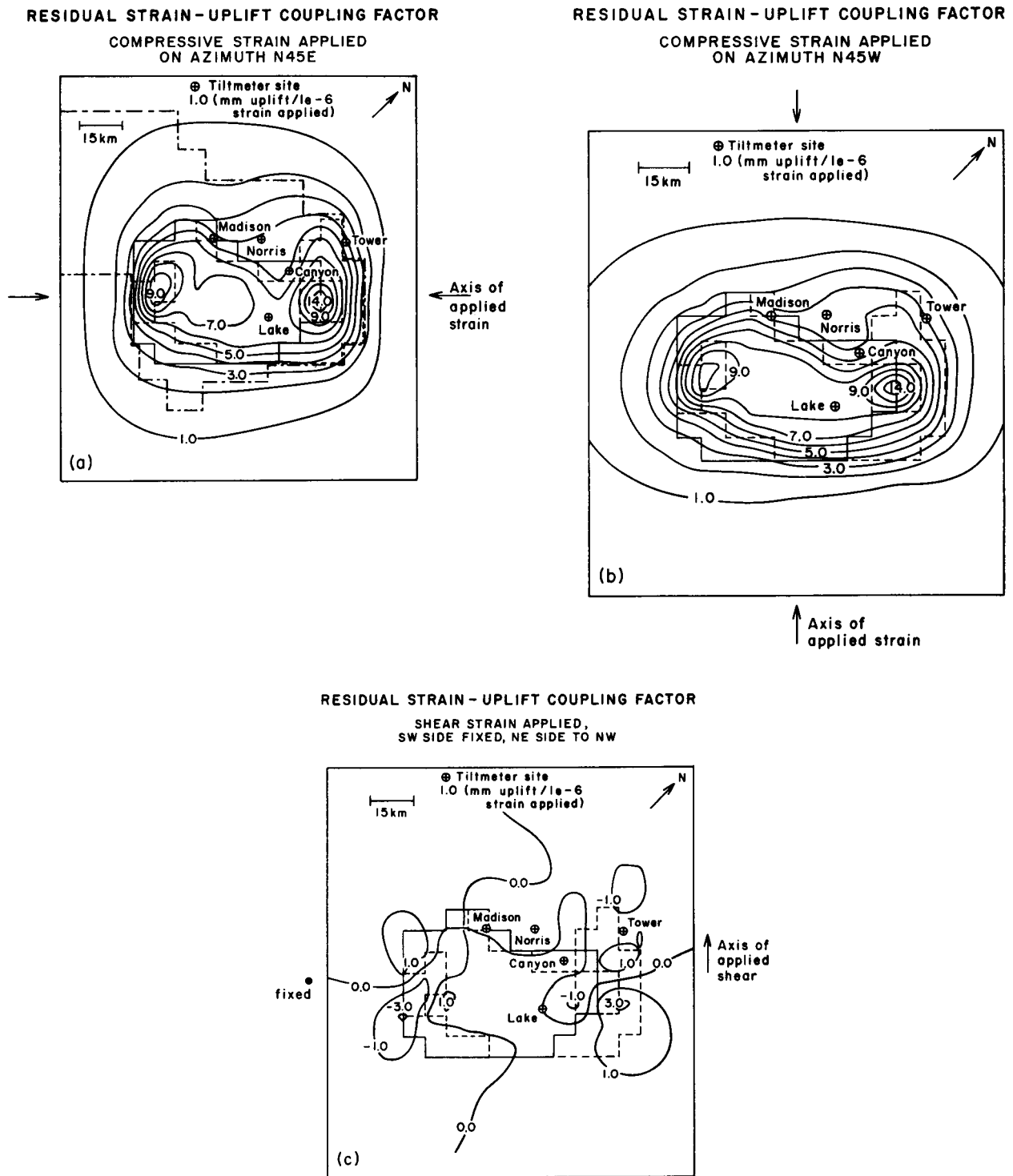


Fig. 4. The strain-uplift coupling factor. The residual uplift predicted by the model after the homogeneous uplift has been subtracted. The uplift is normalized by the applied strain. (a) The result when a compressive strain is applied along an azimuth of  $45^\circ$ , (b) the uplift when the same strain is applied along  $315^\circ$ , and (c) the response to a shear strain applied with the SW side fixed and the NE side shifted in a NW direction. In this and subsequent figures, only the central half of the model containing the anomalous zone is shown. The remainder of the model uses the reference section parameters of Table 5 and extends approximately 60 km in each direction from the edges of the anomalous zone. In these and subsequent figures the boundary of the top layer is shown by solid curves, layer 2 with its low-velocity bodies is shown by dashed curves, and the edge of the anomalous region of the model by long and short dashed curves.

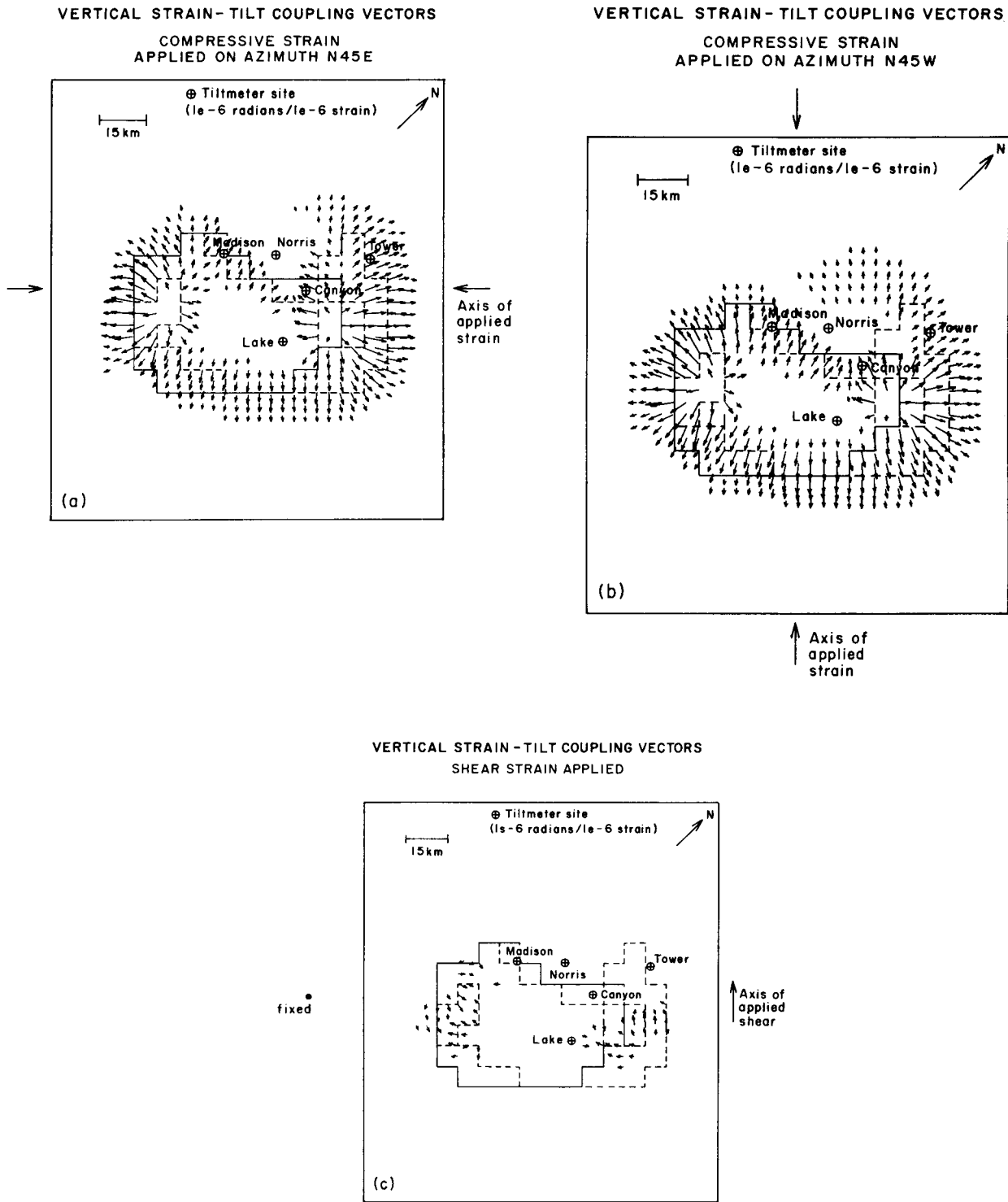


Fig. 5. The strain-vertical tilt coupling vector. These vectors are the vertical derivative of the vertical tilt normalized by the applied strain. (a) The result when a compressive strain is applied along an azimuth of 45°, (b) the same for 315°, and (c) the response to a shear strain.

and one midnode along each vertical boundary. The remaining layers were constructed using rectangular elements with eight nodes, one at each corner. An exploded view of the anomalous elements of the model is shown in Figure 3. The response of the model is dominated by layer 2,

the outline of this layer, the locations of the tiltmeters, and the boundaries of the anomalous zone will be reproduced on the remaining figures for comparison.

The same geometry was used for all of our models; only the elastic parameters were varied

TABLE 6. Comparison of Observations With Sum of Body and Load Tides for Yellowstone National Park Sites

Station	Azimuth, deg	(O)/[(SE) + (OL)]		(O) - [(SE) + (OL)]	
		Amplitude Ratio	Phase, deg	Amplitude Difference, nrad	Phase Difference, deg
Canyon	45	1.00	-10.9	6.3	38
Canyon	315	0.93	-17.2	9.9	137
Tower	45	1.02	-5.8	3.4	50
Tower	315	0.75	-6.0	9.0	86
Lake	45	0.78	-22.9	13.7	0
Lake	315	0.64	+11.0	13.0	51
Madison	45	0.68	+9.9	11.4	-65
Madison	315	0.97	+10.0	6.41	-6
Norris	45	1.16	-28.9	18.4	44
Norris	315	0.54	-49.0	25.6	101

from one model to the next. The various model results differ only in detail, and only a representative model will be discussed below. A detailed discussion of the five models is given by Meertens [1987]. The elastic parameters used to describe the anomalous region for model YEL7C are listed in Table 4; the constants for the low-velocity body in layer 2 are listed as layer 2L. The parameters of the reference section, used for the exterior, are listed in Table 5.

TABLE 7.  $M_2$  Theoretical Strain Tides for Yellowstone National Park

Theory	Azimuth, deg	Amplitude, $10^{-9}$	Phase, deg
Body	45	8.10	-32.8
Body	315	8.10	32.8
Body	Shear	4.64	0.0
Ocean load(s)	45	2.60	138.2
Ocean load(p)	45	3.61	136.4
Ocean load(s)	315	6.94	-30.6
Ocean load(p)	315	9.40	-29.1
Ocean load(s)	Shear	1.13	134.1
Ocean load(p)	Shear	1.28	136.4
Combined	45	5.08	-26.7
Combined	315	8.55	19.3
Combined	Shear	3.88	12.6

Note that (s) uses ocean model of Schwiderski [1980], (p) uses model of Parke [1978]. The combined entry uses the average of the two load estimates.

#### Model Loading

The displacements at each node were determined using program ADINA [Adina Engineering, 1981]. (The name ADINA is used for identification purposes only and no endorsement is implied.) The far-field homogeneous strain is applied on the model boundaries using prescribed displacements. The three independent surface strain components are the two horizontal uniaxial components  $\epsilon_{xx}$  and  $\epsilon_{yy}$  and the horizontal shear strain  $\epsilon_{xy}$ . The horizontal coordinates are x and y; the vertical direction is z, and the displacements in these directions are u, v and w, respectively. The nodes on the vertical sides of the model were allowed to move vertically, and the prescribed displacements were uniform with depth. The nodes on the base of the model are free to move horizontally but are constrained vertically.

#### Model Results

The residual strain-uplift coupling factor, shown in Figure 4, is the uplift (when positive) or subsidence (when negative) induced by the far-field strain minus the first-order homogeneous strain-induced uplift which depends on the thickness and Poisson's ratio of the model. It is normalized by the amplitude of the homogeneous strain which is applied along an azimuth of  $315^\circ$ . The uplift pattern is essentially the same if the strain is applied along an azimuth of  $45^\circ$  because the anomalous body responds primarily to areal strain, which is the sum of the strains applied along the two coordinate azimuths.

The vertical displacement produced by a unit shear is smaller in magnitude and has a more complicated pattern. There is no uniform uplift, and the effect is primarily a rotation due to the heterogeneous nature of the model.

The vertical tilt is the vertical derivative of the horizontal displacement; it is continuous across the vertical sides of the elements. The

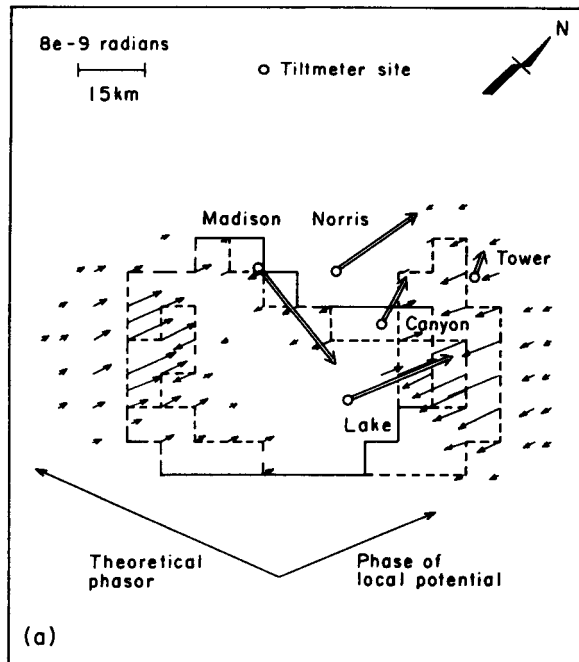
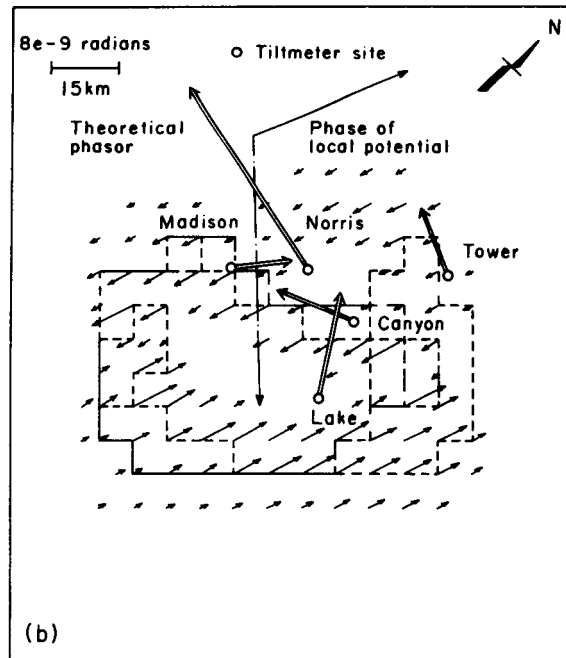
M2 TIDAL STRAIN-TILT COUPLING PHASORS  
VERTICAL TILT, AZIMUTH 45°M2 TIDAL STRAIN-TILT COUPLING PHASORS  
VERTICAL TILT, AZIMUTH 315°

Fig. 6. The tidal tilts as a function of position that result from the application of tidal strain to the finite element model. The length of each vector gives the amplitude of the strain-induced tilt, and the direction gives the phase with respect to the local potential. The homogeneous theoretical phase (body tide + ocean load) is also shown. (a) The effect on a tiltmeter oriented along an azimuth of 45°; (b) the effect along a 315° azimuth.

resulting tilts are normalized by the applied strain and are shown in Figure 5.

The anomalous region also causes a modification to the homogeneous strain field called the residual strain coupling factor. The primary effect of the anomalous body is an increase of up to 40% in the applied uniaxial strain. The enhancement is generally aligned with the applied strain and would substantially affect strain tide measurements. A comparison with a model which has normal elastic constants at the surface shows that much of the surface strain comes from coupling between the surface layer and layer 2.

The residual strain-stress coupling shows the opposite effect, as expected. The stress factors do not follow the outline of the anomalous elements of layer 2. This means that the reduction in compressive stress at the surface due to the presence of the low modulus material is larger than the increase in compressive stress expected due to the increase in contractional strain at the same location.

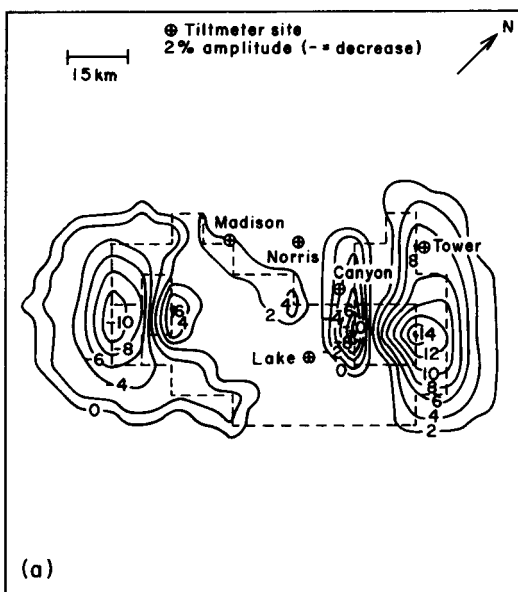
Overall, the anomalous body acts as a weak inclusion embedded in a plate, reproducing the basic features of the Harrison model discussed above. It strains more than the surrounding material, and the stresses induced by the homogeneous external strain are not supported internally but are redistributed to the surrounding material.

## Comparison With Experiment

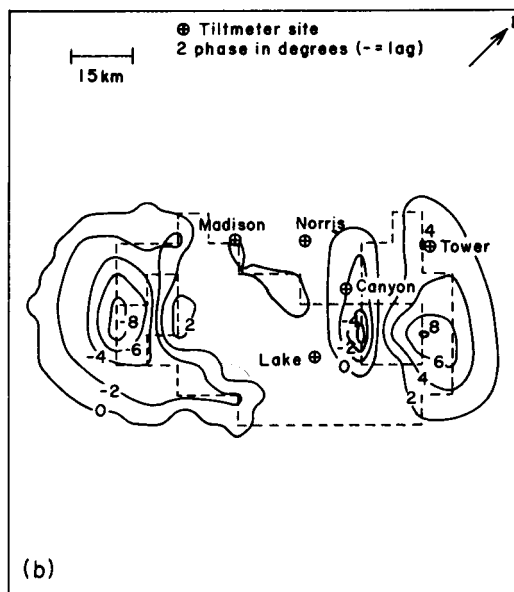
The measured amplitude of the geologic effect ( $G$ ) is the difference between the observed amplitude ( $O$ ), and the sum of the solid earth body tide ( $SE$ ) and the ocean load ( $OL$ ). The correction for local topography is negligible for our locally flat sites [Meertens and Wahr, 1986]. The ratio  $O/[(SE) + (OL)]$  and the difference  $O - [(SE) + (OL)]$ , computed from Tables 2 and 3, are given in Table 6. The deviation of the ratio from unity (or the difference from zero) measures the relative contribution of the caldera (or some other unmodeled effect). The estimate of ( $G$ ) varies considerably from station to station and depends on azimuth. The admittance discrepancy at Canyon is small, but the value elsewhere is 25-50% of sum of the body tide and the ocean load.

The model estimate of ( $G$ ) is derived from the strain-tilt vectors and the tidal strain. The homogeneous applied strain (including the ocean load contribution) is computed along the principal axes of the model. These values, and the associated shear strains, are shown in Table 7. Note that the ocean load contribution to the  $M_2$  strain tide is almost 50% of the body tide, while the corresponding tilt contribution is smaller (Table 3). The resulting tilts from the three applied strains are summed and then resolved

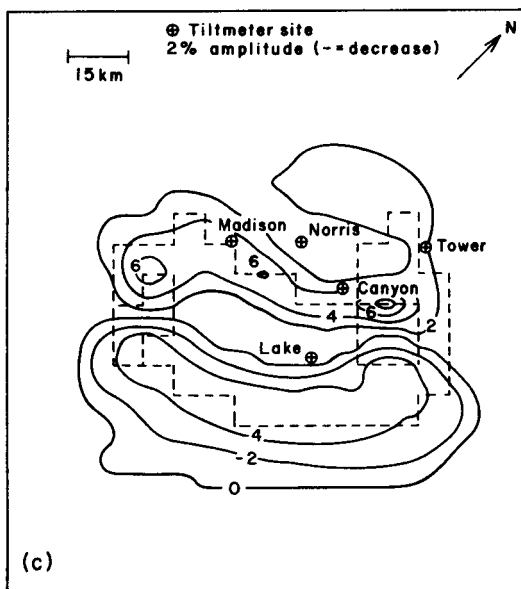
M2 TIDAL GEOLOGICAL EFFECT (amplitude)  
VERTICAL TILT AZIMUTH N45E



M2 TIDAL GEOLOGICAL EFFECT (phase)  
VERTICAL TILT, AZIMUTH N45E



M2 TIDAL GEOLOGICAL EFFECT (amplitude)  
VERTICAL TILT, AZIMUTH N45W



M2 TIDAL GEOLOGICAL EFFECT (phase)  
VERTICAL TILT, AZIMUTH N45W

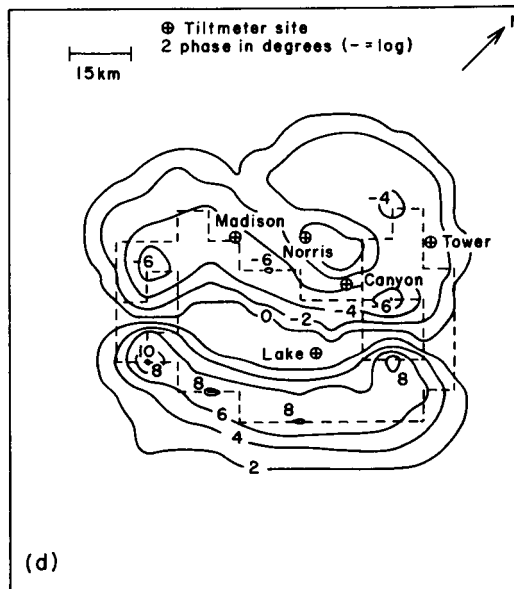


Fig. 7. The amplitude and phase contours of the effect of the anomalous zone on the tilt tides from model YEL7C. The amplitude (expressed as a percent change) and phase (expressed as a phase difference) are shown with respect to the homogeneous tilt tide (body tide + ocean load). (a) and (b) The effect along an azimuth of 45°; (c) and (d) for 315°.

along the principal axes of the model. Figure 6 shows the strain-induced tilt as a phasor at each node. The amplitude and phase of the body tide and the phase of the local potential, both of which are the same for all of the stations, are shown for reference. The tiltmeter estimates of

(G), given by  $(O) - [(SE) + (OL)]$ , are also plotted in Figure 6 for comparison. Figure 7 shows model estimate of (G) as a percentage of  $[(SE) + (OL)]$ .

The maximum amplitude of the strain-induced tilts is 12% of the homogeneous tide. The presence of the NE low-velocity body causes a

## YELLOWSTONE GEODETIC UPLIFT RATES 1923-1975 LINE LEVELING DATA FROM PELTON AND SMITH, 1982

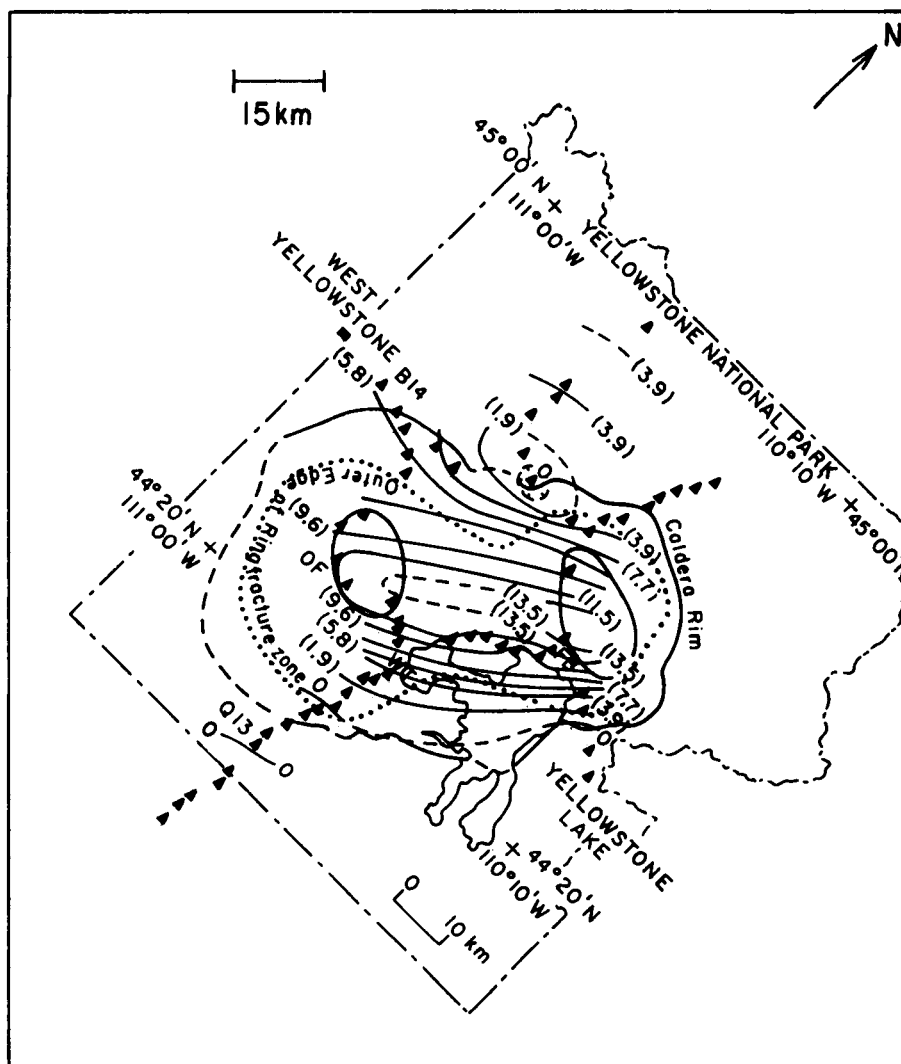


Fig. 8. Contour plot of the observed uplift rates in millimeters per year calculated by differencing the line level surveys of 1975 and 1923.

local phase reversal in the NE tilt component (Figure 6a) but does not significantly alter the NW tilt component (Figure 6b).

### Secular Effects

Figure 8 is a contour plot of the uplift in Yellowstone, obtained by differencing the line level measurements made in 1975 and 1923 [Pelton and Smith, 1982]. The total uplift was 700 mm, averaging 13.5 mm/yr. The spatial pattern of the uplift is similar to Figure 4, and a regional contractional strain with an average magnitude of  $1.5 \times 10^{-6} \text{ yr}^{-1}$  would produce the observed uplift by tilt-strain coupling. A secular contractional strain of this magnitude should be borne out by a study of earthquake focal mechanisms, but such studies show a much more complex stress pattern with significant short-range variation [Doser, 1985].

### Conclusions

We have used an array of deep-borehole tiltmeters to study secular and tidal tilt in Yellowstone National Park, Wyoming. The tides that we measured there differ from the sum of the body tide and the ocean load by up to 50%. Only near a fault zone in Germany have comparably large tilt anomalies been observed. The discrepancy depends both on position and on azimuth and does not vary smoothly across the caldera.

The axially symmetric model of Harrison predicts deviations of up to 40% in the amplitude of the tilt tides (Figure 1), and a model of this type that explained our results could be constructed. It would require a sharp contrast in elastic parameters close to Norris, Madison, and Lake. Neither the location nor the sharp transition are consistent with the other evidence, and the agreement would depend on how the edge singu-

larities of the Harrison model were smoothed.

Instead of smoothing the predictions of a simple model, we have constructed a three-dimensional finite element model of the region incorporating seismic, refraction, and gravity data. The effect on the tides is inevitably smaller than the estimate derived from the Harrison model, since the contrast in material properties is more gradual. The predictions of this model are too small: tidal amplitudes change by 12% or less and the phase shift is 10° or less. More significantly, the predicted spatial variation disagrees with our measurements. We cannot reduce this discrepancy by varying only the elastic properties of the model, and significant changes in the size and position of the anomalous zone would be required to explain our observed spatial distribution. This conclusion could also have been derived in a more qualitative way from an empirically smoothed version of the the Harrison model. The shape and position of the anomalous zone are constrained by previous geophysical measurements, however, and we have not been able to construct a model that explains all of the observations.

The discrepancies between any of the models and the observations are much larger than we observed anywhere else and cannot be explained by any of the sources of error we have considered.

The results are independent of the individual tiltmeters. Except for Norris, at least two different tiltmeters were used at every site, and the same tiltmeter was often removed for repair and then replaced on a different azimuth at the same site.

Tilt measurements are more sensitive to gradients in elastic parameters than the data that defined our finite element model, and the disagreement between the two may indicate a more complex or more rapid spatial variation than is present in the current description of the region.

**Acknowledgments.** We gratefully acknowledge the support of the Air Force Geophysics Laboratory under contracts F-19628-78-C-0065 and F-19628-81-K-0040. We are also very grateful to the Superintendent of Yellowstone, to Wayne Hamilton, the scientific coordinator, and to the many area rangers who allowed us to work in the park and were very helpful in many ways. Chris Harrison, formerly of the Department of Geological Sciences of the University of Colorado, also worked on the initial stages of the project and provided useful advice throughout the work. J. L. is a staff member of the NBS Time and Frequency Division.

#### References

- Adina Engineering, A finite element program for automatic dynamic incremental and linear analysis, Rep. AE 81-1, Watertown, Mass., 1981.
- Beaumont, C., and J. Berger, Earthquake prediction: Modification of the Earth tides and strains by dilatancy, Geophys. J. R. Astron. Soc., 39, 111-121, 1974.
- Bogy, D. B., Edge-bonded dissimilar orthogonal elastic wedges under normal and shearing load, J. Appl. Mech., 35, 460-466, 1968.

- Christensen, R. M., Mechanics of Composite Materials, John Wiley, New York, 1979.
- Daniels, R. G., and D. M. Boore, Anomalous shear wave delays and surface wave velocities at Yellowstone caldera, Wyoming, J. Geophys. Res., 87, 2731-2744, 1982.
- Doser, D. I., Source parameters and faulting processes of the 1959 Hebgen Lake, Montana, earthquake sequence, J. Geophys. Res., 90, 4537-4556, 1985.
- Eaton, G. P., R. L. Christiansen, H. M. Iyer, A. M. Pitt, D. R. Mabey, H. R. Blank, Jr., I. Zietz, and M. E. Gettings, Magma beneath Yellowstone National Park, Science, 188, 787-796, 1975.
- Evoy, J. A., and R. B. Smith, Releveling and microgal gravity reobservations: An evaluation of these techniques for delineating buried thermal bodies, final technical report for grant 14-08-0001-G-438, U.S. Geol. Surv., Menlo Park, Calif., 1979.
- Harrison, J. C., Implications of cavity, topographic and geologic influences on tilt measurements, Proceedings of 9th Geophysics Conference, report, pp. 283-287, Ohio State Univ., Dep. of Geod. Sci., Columbus, 1978.
- Harrison, J. C., and D. Flach, Eine Betrachtung der Erdezeiten, paper presented at 36th Meeting, German Geophys. Soc., Bochum, 1976.
- Iyer, H. M., Deep structure under Yellowstone National Park, U.S.A.: A continental "hot spot," Tectonophysics, 56, 165-197, 1979.
- Iyer, H. M., J. R. Evans, G. Zandt, R. M. Stewart, J. M. Cookley, and J. N. Roloff, A deep low velocity body under the Yellowstone caldera, Wyoming; Delineation using teleseismic P-wave residuals and tectonic interpretations: Summary, Geol. Soc. Am. Bull., 92, 1471-1646, 1981.
- Lehman, J. A., R. B. Smith, M. M. Schilly, and L. W. Braille, Crustal structure of the Yellowstone caldera from delay time analyses and correlation with gravity correlations, J. Geophys. Res., 87, 2713-2730, 1982.
- Levine, J., C. Meertens, and R. Busby, Tilt observations using borehole tiltmeters, 1, Analysis of tidal and secular tilt, J. Geophys. Res., this issue.
- Meertens, C., Tilt tides and tectonics at Yellowstone National Park, Ph.D. thesis, Univ. of Colo., Boulder, 1987.
- Meertens, C., and J. M. Wahr, Topographic effect on tilt, strain and displacement measurements, J. Geophys. Res., 91, 14,057-14,062, 1986.
- Parke, M. E., Open ocean tide modeling, Proceedings of 9th Geophysics Conference report, pp. 289-297, Ohio State Univ., Columbus, 1978.
- Pelton, J. R., and R. B. Smith, Recent crustal uplift in Yellowstone National Park, Science, 206, 1179-1182, 1982.
- Schwiderski, E. W., On charting global ocean tides, Rev. Geophys., 18, 243-268, 1980.
- Smith, R. B., and L. W. Braille, Crustal structure and evolution of an explosive silicic volcanic system at Yellowstone

- National Park, in Explosive Volcanism: Inception, Evolution and Hazards, pp. 96-109, National Academy Press, Washington, D. C., 1984.
- Smith, R. B., and R. L. Christiansen, Yellowstone Park as a window on the Earth's interior, Sci. Am., 242, 104-117, 1980.
- Smith, R. B., L. W. Braile, M. M. Schilly, J. Anson, C. Prodehl, M. Baker, J. H. Healey, S. Mueller, and R. Greenfelder, The 1978 Yellowstone-eastern Snake River Plain seismic profiling experiment: Crustal structure of the Yellowstone region and experiment design, J. Geophys. Res., 87, 2583-2596, 1982.
- R. Busby, Lamont-Doherty Geological Observatory, Seismology Bldg., Palisades, NY 10964.
- J. Levine, Joint Institute for Laboratory Astrophysics, University of Colorado, Boulder, CO 80309-0440.
- C. Meertens, Department of Geology and Geophysics, 615 W. Browning Bldg., University of Utah, Salt Lake City, UT 84112.

(Received September 22, 1987;  
revised August 29, 1988;  
accepted August 31, 1988.)